Journal of Hydrology (2007) 332, 144–157

available at www.sciencedirect.com

ScienceDirect

journal homepage: www.elsevier.com/locate/jhydrol

Geostatistical interpolation of hourly precipitation from rain gauges and radar for a large-scale extreme rainfall event

Uwe Haberlandt *

Institute of Water Resources Management, Hydrology and Agricultural Hydraulic Engineering, Leibniz University of Hannover, Appelstr. 9A, 30167, Hannover, Germany

Received 20 December 2005; received in revised form 6 June 2006; accepted 16 June 2006

KEYWORDS
Rainfall;
Geostatistics;
Kriging;
Radar

Summary The methods kriging with external drift (KED) and indicator kriging with external drift (IKED) are used for the spatial interpolation of hourly rainfall from rain gauges using additional information from radar, daily precipitation of a denser network, and elevation. The techniques are illustrated using data from the storm period of the 10th to the 13th of August 2002 that led to the extreme flood event in the Elbe river basin in Germany. Cross-validation is applied to compare the interpolation performance of the KED and IKED methods using different additional information with the univariate reference methods nearest neighbour (NN) or Thiessen polygons, inverse square distance weighting (IDW), ordinary kriging (OK) and ordinary indicator kriging (IK). Special attention is given to the analysis of the impact of the semivariogram estimation on the interpolation performance. Hourly and average semivariograms are inferred from daily, hourly and radar data considering either isotropic or anisotropic behaviour using automatic and manual fitting procedures.

The multivariate methods KED and IKED clearly outperform the univariate ones with the most important additional information being radar, followed by precipitation from the daily network and elevation, which plays only a secondary role here. The best performance is achieved when all additional information are used simultaneously with KED. The indicator-based kriging methods provide, in some cases, smaller root mean square errors than the methods, which use the original data, but at the expense of a significant loss of variance. The impact of the semivariogram on interpolation performance is not very high. The best results are obtained using an automatic fitting procedure with isotropic variograms either from hourly or radar data.

* Tel.: +49 511 762 2287; fax: +49 511 762 3731.
E-mail address: haberlandt@iww.uni-hannover.de.

0022-1694/$ - see front matter © 2006 Elsevier B.V. All rights reserved.
doi:10.1016/j.jhydrol.2006.06.028

Introduction

Precipitation data with high-resolution in space and time are needed for distributed hydrological modelling of floods, erosion and other highly non-linear processes. While the spatial resolution of non-recording precipitation networks with daily data are often suitable, this is seldom the case for hourly data or data from shorter time intervals. A reliable spatial estimation of data from shorter time intervals based solely on the sparse gauge networks is, therefore, hardly feasible. Radar data have recently been used more frequently as inputs for hydrological modelling (e.g., Fassnacht et al., 2003; Neary et al., 2004; Tetzlaff and Uhlenbrook, 2005). However, despite the high spatial resolution of radar data there is often a large space–time variable bias in radar rainfall estimates. To provide optimal input for distributed hydrological modelling, the best strategy is probably a combination of all available information on rainfall, including data from hourly point observations, radar data, denser daily measurements, physiographic factors like elevation, and applying sophisticated interpolation or merging methods.

Quite a number of modern interpolation methods have been proposed for rainfall (Dubois et al., 1998). Besides geostatistical approaches, such as ordinary kriging, kriging with external drift and co-kriging (Bárdossy, 1993; Goovaerts, 2000; Lloyd, 2005), other techniques based on splines (Hutchinson, 1998a,b) or genetic algorithms (Demyanov et al., 1998; Huang et al., 1998) have been applied. This paper focuses on multivariate geostatistical approaches with the ability to incorporate additional information into the interpolation procedure. Time invariant elevation data are most frequently used as supplementary information (Goovaerts, 2000; Hevesi et al., 1992a,b). However, the extra value of the elevation information depends on the time step and the type of precipitation considered for interpolation. Generally, the correlation between elevation and precipitation depends on the precipitation mechanism of the event and decreases with increasing time resolution. Using time variant additional information allows the combination of point measurements from rain gauges with other data sources like radar (Ehret, 2002; Seo et al., 1990a,b), satellite data (Grimes et al., 1999) or results from numerical weather prediction models (Haberlandt and Kite, 1998). Special problems occur with the semi-automatic interpolation of whole precipitation time series of daily, hourly or shorter time steps considering varying precipitation properties, such as intensity, spatial dependence structure, correlation with additional information and the fractional spatial coverage of rainfall occurrence (Seo, 1998).

The main objective of the paper is to contribute to a better integration of data from sparsely distributed point rainfall measurements, with data from high-resolution radar patterns, by means of multivariate geostatistical interpolation. It is important to emphasize, that this combination problem is tackled here from the gauge rainfall interpolation point of view and not from the radar rainfall calibration point of view as discussed in, for example, Krajewski and Smith (2002). For the proposed interpolation, the basic assumption required here is that the gauge precipitation is correct and that the radar data provide only extra information. In addition to incorporating radar observations, data from a denser daily precipitation network and elevation data are evaluated as supplementary information.

The paper is organised as follows. After Section 'Introduction', a short description of the multivariate geostatistical methods kriging with external drift and indicator kriging with external drift is given in Section 'Methodology'. Section 'Study region and data' describes the study area and the data with special reference to the pre-processing of radar observations. Section 'Analysis and results' is divided into three subsections dealing with the inference and impact of semivariograms, the assessment of indicator semivariograms and the comparisons of interpolation methods using different additional information. Finally, conclusions are drawn and an outlook is given in Section 'Conclusions'.

Methodology

In this section, a brief introduction is given to the multivariate geostatistical methods used in this study: kriging with external drift and indicator kriging with external drift. The well-known univariate methods, nearest neighbour (NN) or Thiessen polygons, inverse square distance weighing (IDW), ordinary kriging (OK) and ordinary indicator Kriging (IK), which are used as reference, will not be described here. For a detailed description of univariate and multivariate geostatistical interpolation methods the reader is referred to geostatistical textbooks (e.g., Goovaerts, 1997; Isaaks and Srivastava, 1989). The Geostatistical Software Library (Gslib) (Deutsch and Journel, 1992) has been employed here for the computational implementation of the algorithms. Some modifications of the original programs have been made to allow the incorporation of multiple external drifts.

Kriging with external drift

Kriging with external drift (KED) (Ahmed and De Marsily, 1987) allows the processing of non-stationary random functions $Z(\mathbf{u})$ taking into account, simultaneously, the spatial dependence of the variable and its linear relation to one or more additional variables. The intrinsic hypothesis, that the expected value of $Z(\mathbf{u})$ is constant within the domain, is not required anymore. Instead, the expected value of the primary variable is linearly related to m additional variables $Y_k(\mathbf{u})$, $k = 1, \ldots, m$:

$$E[Z(\mathbf{u})|Y_1(\mathbf{u}), Y_2(\mathbf{u}), \ldots, Y_m(\mathbf{u})] = b_0 + \sum_{k=1}^{m} b_k Y_k(\mathbf{u}) \quad (1)$$

where b_0, $b_1, \ldots, b_m$ are unknown constants. Local search windows for the estimation of the unknown point $\mathbf{u}$ imply that the parameters b vary in space. The second assumption, that the variance of the increment $[Z(\mathbf{u}+\mathbf{h}) - Z(\mathbf{u})]$ between two points depends only on the distance vector $\mathbf{h}$ and not on the locations $\mathbf{u}$ and $\mathbf{u} + \mathbf{h}$, still holds:

$$\mathrm{Var}[Z(\mathbf{u}+\mathbf{h}) - Z(\mathbf{u})] = E\left\{[Z(\mathbf{u}+\mathbf{h}) - Z(\mathbf{u})]^2\right\} = 2\gamma(\mathbf{h}) \quad \mathbf{u} \in D \quad (2)$$

Here, $\gamma(\mathbf{h})$ is the semivariogram, which will also be referred to as ''variogram'' in the following text. The linear estimator

for the unknown point $\mathbf{u}_0$ is a weighted sum of the observations from the n surrounding points $\mathbf{u}_i$:

$$Z^*(\mathbf{u}_0) = \sum_{i=1}^{n} \lambda_i Z(\mathbf{u}_i) \tag{3}$$

where λ_i for $i = 1, \ldots, n$ are the weights to be estimated by solving the kriging system:

$$\begin{aligned} &\sum_{j=1}^{n} \lambda_j \gamma(\mathbf{u}_i - \mathbf{u}_j) + \mu_0 + \sum_{k=1}^{m} \mu_k Y_k(\mathbf{u}_i) = \gamma(\mathbf{u}_i - \mathbf{u}_0) \\ &\quad i = 1, \ldots, n \\ &\sum_{j=1}^{n} \lambda_j = 1 \\ &\sum_{j=1}^{n} \lambda_j Y_k(\mathbf{u}_j) = Y(\mathbf{u}_0) \quad k = 1, \ldots, m \end{aligned} \tag{4}$$

The kriging system (4) consists of $n + m + 1$ equations, where n is the number of neighbours considered, m is the number of additional variables Y_k included and μ_k are the $m + 1$ Lagrange parameters. From (4) it can be seen that the coefficients b_k need not to be known explicitly but the additional variables Y_k must be known at all points $\mathbf{u}$.

When kriging with external drift is applied for the spatial interpolation of a whole time series of precipitation, Eqs. (1)–(4) are applied independently for each time step of the series. The coefficients b of (1) will change not only in space, as mentioned above, but also for each time step. Thus, with KED, it is possible to consider a space–time variable connection between precipitation as the primary variable and any additional information. This feature is quite important when radar data are used as an additional variable since it enables the imitation of a space–time variable Z–R relationship between rainfall and reflectivity (cp. Eq. (15)).

Theoretically, the variogram for KED needs to be inferred from the residuals $Z(\mathbf{u}) - m(\mathbf{u})$. This is not straightforward, since neither the residuals nor the trend $m(\mathbf{u})$ is known a priori. One way would be to estimate the trend, $m(\mathbf{u})$, as shown in (1), using a slightly modified KED system of (4) (see Goovaerts, 1997, p. 196), and then calculating the residuals $r(\mathbf{u}) = Z(\mathbf{u}) - m(\mathbf{u})$ and the residual variogram. This would require an iterative process starting, for example, with an approximate variogram, e.g., from $Z(\mathbf{u})$, and improving it subsequently. Another simpler approach would be to select only data pairs that are unaffected by the trend $m(\mathbf{u}) = 0$, which would then allow $Z(\mathbf{u}) = r(\mathbf{u})$ to be used directly for the inference of the residual variogram. If, for instance, the trend were anisotropic, the semivariogram would be estimated only from pairs of z-values perpendicular to the trend direction, assuming isotropic spatial variations of the residuals. The first iterative approach is very demanding and will not be employed here, since interpolations are required for each time step. The experimental variograms will be estimated based on the observed $Z(\mathbf{u})$ data only:

$$\gamma^*(\mathbf{h}) = \frac{1}{2n(\mathbf{h})} \sum_{i=1}^{n(\mathbf{h})} [Z(\mathbf{u}_i) - Z(\mathbf{u}_i + \mathbf{h})]^2 \tag{5}$$

where $n(\mathbf{h})$ is the number of data points, which are located a distance vector $\mathbf{h}$ apart. Uncertainties, resulting from this simplifying assumption will be assessed based on the second approach described above; by comparisons of interpolation results obtained using an isotropic variogram and a variogram estimated solely perpendicular to the trend direction (see Section 'Variogram inference and impact on interpolation').

The combination of a nugget effect with the spherical model is used uniformly for all methods and time steps as a theoretical variogram model:

$$\gamma(\mathbf{h}) = c_0 + \begin{cases} c\left(\frac{3}{2}\frac{h}{a} - \frac{1}{2}\frac{h^3}{a^3}\right) & \text{if} \quad \mathbf{h} \leqslant a \\ c & \text{otherwise} \end{cases} \tag{6}$$

Considering that time series of the primary variable are available, the fitting of the theoretical model $\gamma(\mathbf{h})$ to the experimental one $\gamma^*(\mathbf{h})$ has to be done for each time step, respectively. This can be a very time consuming procedure if long time series with small time increments are used. In this study, two different approaches are taken and compared. First, an average experimental variogram is computed as follows:

$$\bar{\gamma}^*(\mathbf{h}) = \frac{1}{2m} \sum_{t=1}^{m} \frac{1}{n_t(\mathbf{h}) \cdot s_t^2(Z)} \sum_{i=1}^{n_t(\mathbf{h})} [Z(\mathbf{u}_i, t) - Z(\mathbf{u}_i + \mathbf{h}, t)]^2 \tag{7}$$

where m is the number of time steps t and $n_t(\mathbf{h})$ is the number of data pairs separated by the distance vector $\mathbf{h}$ for time step t. Before averaging, the experimental variograms are standardized by the variance s_t^2 for each time step. In this case, only one variogram is finally obtained, for which the fitting of the theoretical model (6) will be done manually. Second, an automatic fitting procedure is applied providing a specific variogram $\gamma_t(\mathbf{h})$ for each time step t such that the weighted sum of squares between the experimental and the theoretical variogram approaches a minimum (Cressie, 1985):

$$\sum_{k=1}^{K} \frac{n_t(\mathbf{h}_k)}{\gamma_t^2(\mathbf{h}_k)} \cdot [\gamma_t^*(\mathbf{h}_k) - \gamma_t(\mathbf{h}_k)]^2 \rightarrow \text{Min} \tag{8}$$

This gives more importance to the smaller lags and the ones computed from more data pairs. The minimisation of Eq. (8) is done using the Nelder and Mead optimisation method (see e.g., Press et al., 1989) assuming that $s_t^2 = c_0 + c$. Thus, only two parameters, the range a and the ratio c_0/c, need to be estimated for the theoretical model represented by Eq. (6) to provide a sufficiently robust optimisation procedure.

Indicator kriging with external drift

For indicator kriging, the observed variable $Z(\mathbf{u})$ is first transformed into a binary indicator variable $I_\alpha(\mathbf{u})$ according to

$$I_\alpha(\mathbf{u}) = \begin{cases} 1 & \text{if} \quad Z(\mathbf{u}) \leqslant \alpha \\ 0 & \text{otherwise} \end{cases} \tag{9}$$

Using several thresholds α_k with $k = 1, \ldots, K$ gives a vector of indicator variables. The interpolation for indicator kriging with external drift (IKED) is done for each indicator using the KED framework, which gives an estimation of the cumulative probability density (cdf) function of $Z(\mathbf{u})$. Order relation deviations are corrected a posteriori following the approach of Deutsch and Journel (1992, p. 81). An estimate of the primary variable $Z(\mathbf{u})$ is obtained using the mean of the cdf, which can be approximated by the following, so-called E-type estimate:

$$Z_E^*(\mathbf{u}) = \sum_{k=1}^{K+1} \frac{\alpha_k + \alpha_{k-1}}{2} \cdot [I_{\alpha_k}^*(\mathbf{u}) - I_{\alpha_{k-1}}^*(\mathbf{u})] \quad (10)$$

where α_k, $k = 1, \ldots, K$ are the specified thresholds and $\alpha_0 = z_{\min}$, $\alpha_{K+1} = z_{\max}$ are the minimum and the maximum values of the Z-Range.

Theoretical and experimental indicator semivariograms are calculated using Eqs. (6) and (7), respectively, as for variogram estimation with untransformed data. However, variograms have to be inferred separately for all indicator variables. Automatic variogram fitting is not applied for indicator variograms, since manual fitting allows easier control over the parameters. The indicator variogram parameters should gradually change from one threshold to the next in order to reduce the occurrence of order relation problems (Deutsch and Journel, 1992, p. 79). Note that when many elements from a time series are interpolated in space, the absolute thresholds and thus the required indicator variograms might differ for each time step. This problem is solved by calculating a set of average indicator variograms at a wide range of fixed absolute thresholds considering the frequency distributions of the primary variable over all time steps. Interpolation is then carried out at relative thresholds based on probability levels using each a predefined variogram that is closest to the actual threshold (see also Section 'Assessment of indicator variograms').

The main motivation to apply IKED here is the possibility to consider a quasi non-linear relationship between the expected value of the primary variable $E[Z(\mathbf{u})]$ and the additional information $Y_k(\mathbf{u})$ through the stepwise implicit application of (1) for different indicators I_α.

Performance assessment

Cross-validation is applied to compare the prediction performances of the univariate and multivariate interpolation methods among one another. In the procedure, the rainfall is estimated successively for each sampled location using the known neighbours but always discarding the observed value for the specific target location (refer to Isaaks and Srivastava, 1989). The observed values $Z(\mathbf{u})$ are then compared with the interpolated ones $Z^*(\mathbf{u})$ using the following performance measures:
the bias

$$\text{Bias} = \frac{1}{n} \sum_{i=1}^{n} [Z^*(\mathbf{u}_i) - Z(\mathbf{u}_i)] \quad (11)$$

the root mean square error normalised with the observed average

$$\text{RMSE} = \frac{1}{\bar{Z}} \cdot \sqrt{\frac{1}{n} \sum_{i=1}^{n} [Z^*(\mathbf{u}_i) - Z(\mathbf{u}_i)]^2} \quad (12)$$

and the coefficient of correlation

$$\text{Cor} = \frac{\text{Cov}[Z(\mathbf{u}), Z^*(\mathbf{u})]}{\sqrt{\text{Var}[Z(\mathbf{u})] \cdot \text{Var}[Z^*(\mathbf{u})]}} \quad (13)$$

Interpolation usually leads to a smoothing of the observations and thus to a loss of variance. Considering the modelling of floods, erosion or other highly non-linear hydrological processes, the smoothing effect in the precipitation data are not wanted. To assess the ability of the interpolation method to preserve the variance, the ratio of the variance of estimated values to the variance of observed values is used as an additional performance criterion:

$$\text{RVar} = \frac{\text{Var}[Z^*(\mathbf{u})]}{\text{Var}[Z(\mathbf{u})]} \quad (14)$$

The closer RVar approaches 1, the better the ability of the interpolation method to preserve the observed variance.

Study region and data

The study region covers an area of about 25,000 km^2 in South-East-Germany and includes the left tributaries of the Obere Elbe river, the Mulde and the Weiße Elster river basins (Fig. 1). Daily precipitation data from 281 non-recording stations, hourly data from 21 recording stations and radar observations from three locations have been used.

The geostatistical techniques are illustrated using data from the storm period of the 10th to the 13th of August 2002, which led to the extreme flood event in the Elbe river basin in Germany. The trigger of the storm event was a typical, so-called Vb depression, which provided a strong persistent supply of moist air from the Mediterranean Sea. Rudolf and Rapp (2003) estimated the contribution of stratiform rainfall and convective rainfall in the ratio of 2 to 1 with additional orographic lifting, which has probably doubled the precipitation amount.

Daily precipitation statistics for the 4 days are provided in Table 1 and hourly precipitation sums for a typical station are shown in Fig. 2. Most precipitation occurred on the 12th of August 2002 with maximum observed precipitation of 312 mm/d for the station Zinnwald. Hourly precipitation was quite variable in space and time comprising several periods with no precipitation at one or more stations. In addition, Table 2 shows a comparison of precipitation statistics from recording stations, non-recording stations and radar cells for the rainfall sum over the total event. It can bee seen that the event statistics between recording and non-recording networks are comparable while the statistics from the radar data show significant underestimations.

Radar observations from three C-band instruments operating at a wavelength of 5 cm and a frequency of 6 GHz are used (DWD, 2002). The data are provided as raw reflectivities Z_r with a spatial polar resolution of 1 km $\times$ 1° azimuth and a time discretisation of 5 min. In a first step, the registration time between radar and gauge data have been synchronised to central European time (CET = UTC + 1 h). Then the data are transformed into rainfall intensities R by the following Z—R relationship, which is the standard equation proposed by the German Weather Service (DWD, 2002):

$$Z_r = 256 \cdot R^{1.42} \quad (15)$$

where Z_r is the reflectivity in mm^6/m^3 and R the rainfall intensity in mm/h. The 5 min time step data for Z_r and R are then averaged each over 12 time steps to obtain mean hourly reflectivities and intensities. Both, original reflectivities Z_r and transformed rainfall rates R are used later as additional information in the interpolation process.

No a priori information was available about local obstructions (ground clutter), which may result in non-meteorological echoes. Thus, a simple procedure has been applied to

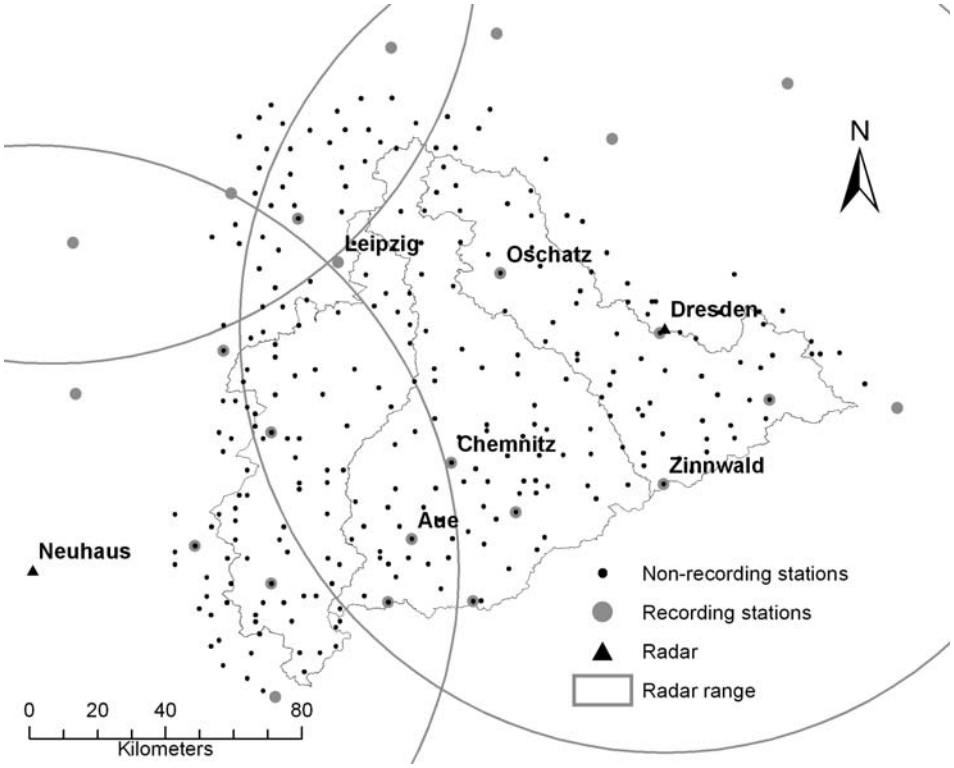

Figure 1 Study region with precipitation stations, radar locations and main river basins: Weiße Elster (left), Mulde (middle) and left tributaries to the Obere Elbe (right) (For the radar station Ummendorf located north-west of the region only the relevant range is shown.).

Table 1 Precipitation statistics of the 281 daily stations for the 4 single days of the event (collection period each from 7.30 h actual day to 7.30 h the following day)

Day	Average (mm/d)	Standard deviation (mm/d)	Minimum (mm/d)	Maximum (mm/d)
10/08/2002	4.8	6.3	0.0	29.0
11/08/2002	28.8	20.3	2.8	106.0
12/08/2002	86.3	62.9	10.0	312.0
13/08/2002	4.4	6.8	0.0	33.6

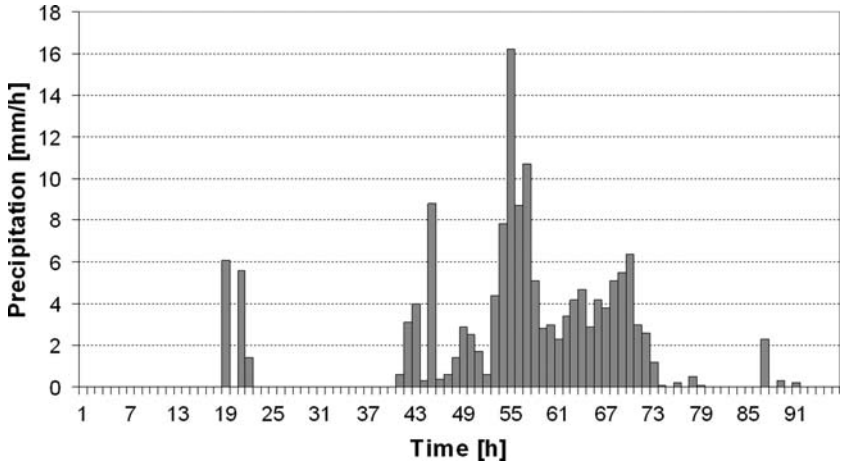

Figure 2 Time series of hourly precipitation for the station Aue from 10/08/2002, 0.00 h to 13/08/2002, 24.00 h.

Table 2 Comparison of precipitation statistics from non-recording stations, recording stations and radar cells for the rainfall sum over the total event from the 10th to the 13th of August 2002 (time periods for non-recording stations from 7.30 to 7.30 h and for recording stations and radar observations from 0.00 to 24.00 h)

Data source	Number of stations/cell values	Average (mm/4d)	Coefficient of variation (−)	Minimum (mm/4d)	Maximum (mm/4d)
Recording stations	21	116.4	0.76	29.0	406.2
Non-recording stations	281	124.3	0.53	39.3	406.2
Radar cells[a]	14,436	37.8	0.37	11.8	102.4

[a] Statistics for pre-processed data within the basin boundaries (errors corrected and interpolated on a rectangular raster, for details see text).

remove these errors from the data. Ground clutter can be recognised from timely permanent echoes accumulating into unusually high quantities of total rainfall. The following two empirical rules were automatically applied after some visual and statistical pre-processing. A radar pixel k is removed from the data sets if

$$R_{\mathrm{tot},k} > \bar{R}_{\mathrm{tot}} + 5 \cdot s(R_{\mathrm{tot}}) = 145 \text{ mm} \quad \text{with} \quad R_{\mathrm{tot},k} = \sum_{t=1}^{m} R(t,k) \cdot \Delta t \tag{16}$$

or if

$$\sum_{t=1}^{m} I_k > 85 \quad \text{with} \quad I_k = \begin{cases} 1 & \text{for } R_{t,k} > 0 \\ 0 & \text{otherwise} \end{cases} \tag{17}$$

where $R_{\mathrm{tot},k}$ is the radar rainfall sum of pixel k, $s(R_{\mathrm{tot}})$ the standard deviation of R_{tot}, I_k an indicator and $m = 96$ time steps. The first rule (16) identifies pixels with unusually high quantities of rainfall and the second rule (17) detects pixels with unusually long rainfall durations, each compared to the precipitation statistics of this event in the study area. The cut-off value of 145 mm in (16) is significantly smaller than the maximum observed rainfall sum from the station networks because of the strong underestimation by radar (cp. Table 2). Note that this cut-off value was calculated from statistics of the raw radar data while the information in Table 2 is based on corrected and interpolated radar data. All together about 1% of all radar pixels have been removed by this procedure. The radar data on polar coordinates were interpolated to a 1 km × 1 km rectangular grid using inverse square distance weighing considering two neighbours in each quadrant. For this procedure all three radar locations with overlapping ranges were included simultaneously. This interpolation represents, in fact, an aggregation procedure here that leads to a reduction of the number of data points from about 19,000 radar pixels to about 14,400 raster cells within the basin boundaries. The application of the simple inverse square distance weighting method was considered appropriate for that purpose.

Analysis and results

Variogram inference and impact on interpolation

One special problem for geostatistical interpolation of whole time series is the effective and reliable estimation of the variograms for each time step. This section discusses the impact of different approaches for the estimation of the semivariogram on the interpolation performance for hourly rainfall data. Hourly and average semivariograms are inferred from daily, hourly and radar data considering either isotropic or anisotropic behaviour using automatic and manual fitting procedures. Table 3 lists the eight different variogram estimation approaches and the parameters that are compared here.

First, as the simplest version without using any data, a linear isotropic variogram with $\gamma(\mathbf{h}) = \mathbf{h}$ is assumed (#1). Next, daily data from 281 non-recording stations are employed for variogram assessments through the calculation of an average experimental variogram according to Eq. (7) and visual fitting. Two cases are distinguished here: one with assumed isotropy (#2) and the other one where anisotropy is taken into consideration (#3). Fig. 3, #2 shows the isotropic version of the variogram from daily data. The permanent increase of the experimental variogram suggests a drift, which is confirmed later in the anisotropic case and for the other variograms. The drift has been ignored when fitting a theoretical model for this and all the other cases, but will be taken into account through the interpolation approaches. Comparing variograms for different directions has shown zonal anisotropy (i.e., varying sill with direction) of daily rainfall, which is modelled as the sum of an isotropic model $g_1(|\mathbf{h}|)$ and a zonal anisotropic model $g_2(\mathbf{h}_\phi)$ depending only on the distance $\mathbf{h}_\phi$ in the direction of greater variance (see Goovaerts, 1997, pp. 93–95):

$$g(\mathbf{h}) = g_1(|\mathbf{h}|) + g_2(\mathbf{h}_\varphi) \tag{18}$$

Here, the direction of greater variance and higher sill has an azimuth angle of $\phi = 90°$ (measured clockwise from north), which is the main wind direction (West–East). The range in that direction of the model $g_2(.)$ is estimated at $a_\varphi = 140$ km (see Table 3). Fig. 3, #3 shows the combined model $g(\mathbf{h})$ and the isotropic model $g_1(|\mathbf{h}|)$ with the experimental variograms estimated for $\phi = 90° \pm 22.5°$ and $\theta = 0° \pm 22.5°$, respectively. The drift is present only in the W–E direction. In addition, the experimental and theoretical variograms for the directions $\phi = 45° \pm 22.5°$ and $\theta = 135° \pm 22.5°$ are shown confirming the validity of Eq. (18) with the assumption of major and minor continuity at directions 0° and 90°, respectively.

Considering hourly station data, only 21 locations for variogram estimation were available. An average experimental variogram (#4) is calculated from Eq. (7) and automatic

Table 3 Variogram types and parameters applied for comparisons

No.	Data source	Fitting method	Anisotropy	Nested structures	Nugget[a]	Sill[a,b]	Range[b] (km)
1	No	Assumed	No	1	0.0	—	—
2	Daily	Average	No	1	0.1	0.9	90
3	Daily	Average	Yes	2	0.1	0.6/0.8	80/140
4	Hourly	Average	No	1	0.4	0.6	80
5	Hourly	Automatic	No	1	Variable	Variable	Variable
6	Radar	Average	No	1	0.2	0.7	50
7	Radar	Average	Yes	2	0.2	0.45/0.55	40/90
8	Radar	Automatic	No	1	Variable	Variable	Variable

#1 Linear model without sill.
#2—#8: Nugget + spherical models (see Eq. (6)).
[a] Nugget and sill are standardized by the variance of the data.
[b] The 1st value is the sill/range for the isotropic component $g_2(|\mathbf{h}|)$; the 2nd value is the sill/range for the zonal structure $g_2(\mathbf{h}_\phi)$; the range for the zonal model in the direction of lower sill is set to a very large value.

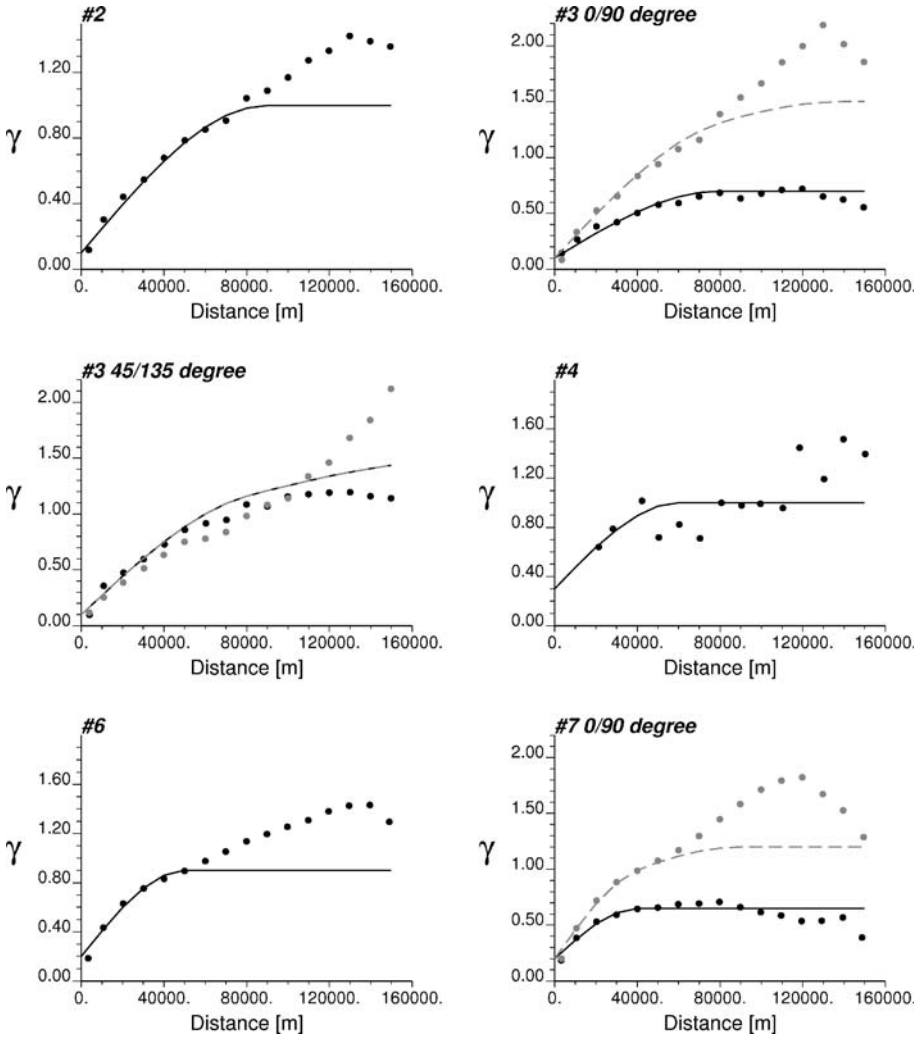

Figure 3 Average standardised variograms characterising hourly rainfall of the extreme storm event based on different data sources and assumptions. The numbers at the top of the *y*-axis indicate the case corresponding to the numbering in Table 3.

variograms (#5) are fitted according to Eq. (8). In both cases, only time steps with significant average precipitation, $\bar{P} \geqslant 0.1$ mm/h were used, which was the case for 64 out of 96 time steps. The variogram was replaced by the average one for each time step where automatic fitting did not converge or resulted in a very large objective func-

tion value. Anisotropy has not been taken into consideration for hourly data because of the small sample size. Fig. 3, #4 shows the average isotropic experimental variogram and the fitted theoretical model for hourly data. Compared to the isotropic daily case, the nugget is higher and the range is shorter.

Finally, hourly radar rainfall rates were used for variogram assessment. Only a subset of the available radar points was utilised here in order to facilitate fast computing in particular with respect to automatic variogram fitting for several time steps. Tests with different numbers of points have revealed that a random sample of 1000 radar cells drawn from within the basin boundaries (see Fig. 1) represents the spatial data structure sufficiently. Three cases with radar data are compared: an average isotropic variogram (#6), an average anisotropic variogram (#7), both calculated from Eq. (7), and an automatic fitting approach (#8) minimizing Eq. (8). Both the isotropic fitted variogram model (Fig. 3, #6) and the anisotropic one (Fig. 3, #7) are similar to the daily variograms, also showing a drift but with higher nugget and smaller range parameters. Compared to the hourly variogram, based on surface observations, both nugget and range parameters are smaller. For automatic fitting using radar data the same rules were applied as for the hourly station data.

In order to assess the impact of the selected variogram model on the prediction performance a cross-validation exercise with the two interpolation methods ordinary kriging (OK) and kriging with external drift (KED) has been carried out. For the latter method, the rainfall sum over the event P_{ev} interpolated from the denser daily network was used as the external drift variable. A local search has been used selecting each the nearest 8 stations for OK and the nearest 16 stations for KED. Using a smaller number of stations for OK leads to a smaller search neighbourhood and thus allows for local departures from the required stationarity of the mean over the area. For the non-stationary-method KED this restriction is not necessary. On the contrary, considering a robust implicit assessment of Eq. (1) and the larger number of constraints on the kriging weights in (4), the number of stations involved should be larger than for univariate kriging methods. The above decision was also supported by some prior tests based on cross-validation using OK and KED with different numbers of neighbours. Table 4 shows the results of the cross-validations applied for all time steps with average precipitation of $\bar{P} \geqslant 0.1$ mm/h using the normalised root mean square error RMSE (12) as the performance criterion.

The semivariogram model has a small impact on prediction performance. However, the use of an assumed linear variogram is not recommended, because this shows by far the largest RMSE values for both interpolation methods. Using variograms from hourly data leads to smaller errors than using variograms from daily data, which is plausible considering the hourly target time step. Although anisotropy is clearly present in the data, no significant differences in prediction performance between isotropic and anisotropic variograms could be found. For KED, in the anisotropic case, only the variogram in the North–South direction without trend is applied, which corresponds to the variogram based on the residuals $r(\mathbf{u})$. This gave no difference in interpolation performance compared to using the isotropic variogram based on $Z(\mathbf{u})$. It can, therefore, be confirmed that the simplifying assumption from Section 'Kriging with external drift' on the use of the original Z data instead of the residuals for variogram inference is applicable. The use of time-specific variograms that are fitted automatically improves little over the use of an averaged semivariogram. The same trend is displayed by the two interpolation methods OK and KED. However, the KED method produces smaller absolute errors and seems generally less sensitive to the choice of the variogram approach. It is obviously sufficient to use an averaged variogram for the rainfall interpolation of this event considering the small absolute error differences. This may, however, not be advisable for longer time series involving different meteorological conditions like frontal systems and convective storms. Nevertheless, even in this event, the variogram parameters automatically fitted over all time steps vary considerably (see Fig. 4). In the following comparisons of different interpolation methods, the averaged isotropic hourly variogram (#4) is used for all OK and KED interpolation approaches.

Table 4 Standardized root mean square error (RMSE) from cross-validation of hourly rainfall using different variograms for time steps with $\bar{P} \geqslant 1.0$ mm/h during the period from the 10th to 13th of August 2002

No.	Variogram type	OK	KED (P_{ev})
1	Assumed linear	1.20	1.02
2	Averaged isotropic daily	1.14	0.99
3	Averaged anisotropic daily[a]	1.13	0.99
4	Averaged isotropic hourly	1.12	0.98
5	Automatic isotropic hourly	1.11	0.97
6	Averaged isotropic radar	1.12	0.98
7	Averaged anisotropic radar[a]	1.12	0.98
8	Automatic isotropic radar	1.10	0.97

[a] For KED only the variogram in N–S direction perpendicular to the trend direction is used.

Assessment of indicator variograms

Hourly indicator variograms are required for indicator kriging of the rainfall time series. Following from the results and the decision made in Section 'Variogram inference and impact on interpolation', average isotropic indicator variograms are calculated using hourly station data based on Eq. (7). Again, only time steps with significant precipitation $\bar{P} \geqslant 0.1$ mm/h were used (64 out of 96 time steps). Absolute thresholds at rainfall rates $\tau = 0.1$, 0.5, 1.0, 2.0, 3.0, 4.0, 6.0, 8.0, 10.0 mm/h were defined for the estimation of nine average experimental indicator variograms. Theoretical variogram models of type (6) have been fitted visually considering a gradually change of the variogram parameters from one threshold value to the next one.

Table 5 lists the estimated parameters and Fig. 5 shows the experimental and fitted theoretical indicator variograms. On comparing the indicator variograms, a decrease in range values and an increase in relative nugget values with rising thresholds can be observed. This indicates a

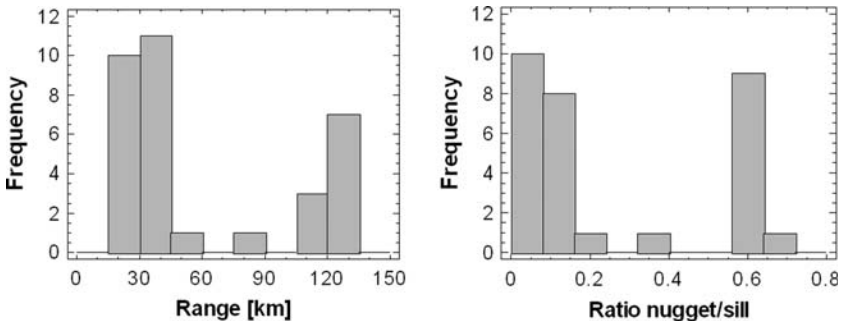

Figure 4 Frequency distributions of the two automatically fitted variogram parameters range and ratio of nugget to sill for time steps with $\bar{P} \geqslant 0.1$ mm/h during the period from the 10th to the 13th of August 2002 (for $n = 33$ h).

smaller spatial persistence of extreme values, which is a quite typical behaviour for environmental variables (e.g., Goovaerts, 1997, p. 323). For interpolation these nine predefined indicator variograms are applied considering the variable frequency of rainfall rates. Relative thresholds from 13 quantiles with non-exceedance probabilities of $p = 0.01$, 0.05, 0.1, 0.2, 0.3, 0.4, 0.5, 0.6, 0.7, 0.8, 0.9, 0.95, 0.99 were used to obtain variable absolute thresholds α_p for each time step. Interpolation is always done for 13 indicator variables based on these thresholds α_p. For each interpolation an indicator variogram is selected for which the distance between interpolation threshold α_p and the threshold τ used for variogram inference, is minimal.

Interpolation using different additional information

Interpolation of hourly precipitation is evaluated focusing on the two multivariate methods kriging with external drift (KED) and indicator kriging with external drift (IKED). As reference, the univariate methods nearest neighbour (NN) or Thiessen polygons, inverse square distance weighing (IDW), ordinary kriging (OK) and ordinary indicator kriging (IK) were also applied. Cross-validations were carried out for performance comparisons based on the criteria defined in Section 'Performance assessment'. Only time steps with average precipitation of $\bar{P} \geqslant 0.1$ mm/h were considered from the whole storm period (33 out of 96 time steps).

Table 5 Parameters of the fitted theoretical indicator variogram models

No.	Threshold (mm/h)	Nugget	Sill	Range (km)
1	0.1	0.20	0.90	140
2	0.5	0.30	0.80	130
3	1.0	0.40	0.70	130
4	2.0	0.40	0.65	130
5	3.0	0.40	0.60	110
6	4.0	0.40	0.50	100
7	6.0	0.40	0.30	80
8	8.0	0.30	0.30	60
9	10.0	0.20	0.30	40

The number of neighbours involved for interpolation has been restricted to the nearest 4, 8 and 16 for IDW, with one station in each quadrant, univariate kriging and multivariate kriging, respectively. For the kriging methods a local search radius without restrictions in direction is used (for discussion see Section 'Variogram inference and impact on interpolation').

First, interpolation methods were compared without using radar information. Table 6 lists the cross-validation results. For the univariate methods, the errors decrease in the order NN, IDW, OK, IK. However, IK is weakest in terms of variance preservation and bias. The multivariate methods KED and IKED show better interpolation performance than the univariate ones. The most important additional information is the rainfall sum over the event P_{ev} interpolated from the denser daily network. This demonstrates a simple but effective way to combine hourly, small time increment data (only available for a few points in space i.e., 21 stations), with daily, time step data (observed at many more locations i.e., 281 stations). Elevation data, El, only provide improvements for interpolation performance if P_{ev} is not available. The reason could be that the rainfall sum calculated from the dense daily network contains sufficient information about the topography of the region. Applying the indicator approach IKED instead of KED does not lead to smaller errors here and shows again the largest loss of variance. Disadvantage of the KED methods is the occurrence of a few negative estimates for some time steps. Those unrealistic values have been simply set to zero before the performance is evaluated (see Deutsch and Journel, 1992, p. 106).

In the second step, radar data were utilised. A direct comparison between radar rainfall and station rainfall was carried out prior to the evaluation of the interpolation approaches. Note, that point rainfall data from surface observations are compared here with block rainfall converted from radar volume scan reflectivity data above the ground. This causes a scale compatibility problem, which inserts additional scatter into the relationship between station and radar rainfall. Fig. 6 shows a direct comparison of hourly rainfall rates from surface observations P for selected stations, with rainfall from radar data R. The strength of the relationship varies with coefficients of determination between 0.59 and 0.89. From the slope of the regression lines it is clear that the gauge rainfall is about 3–10 times higher than the radar rainfall. In addition, Fig. 7

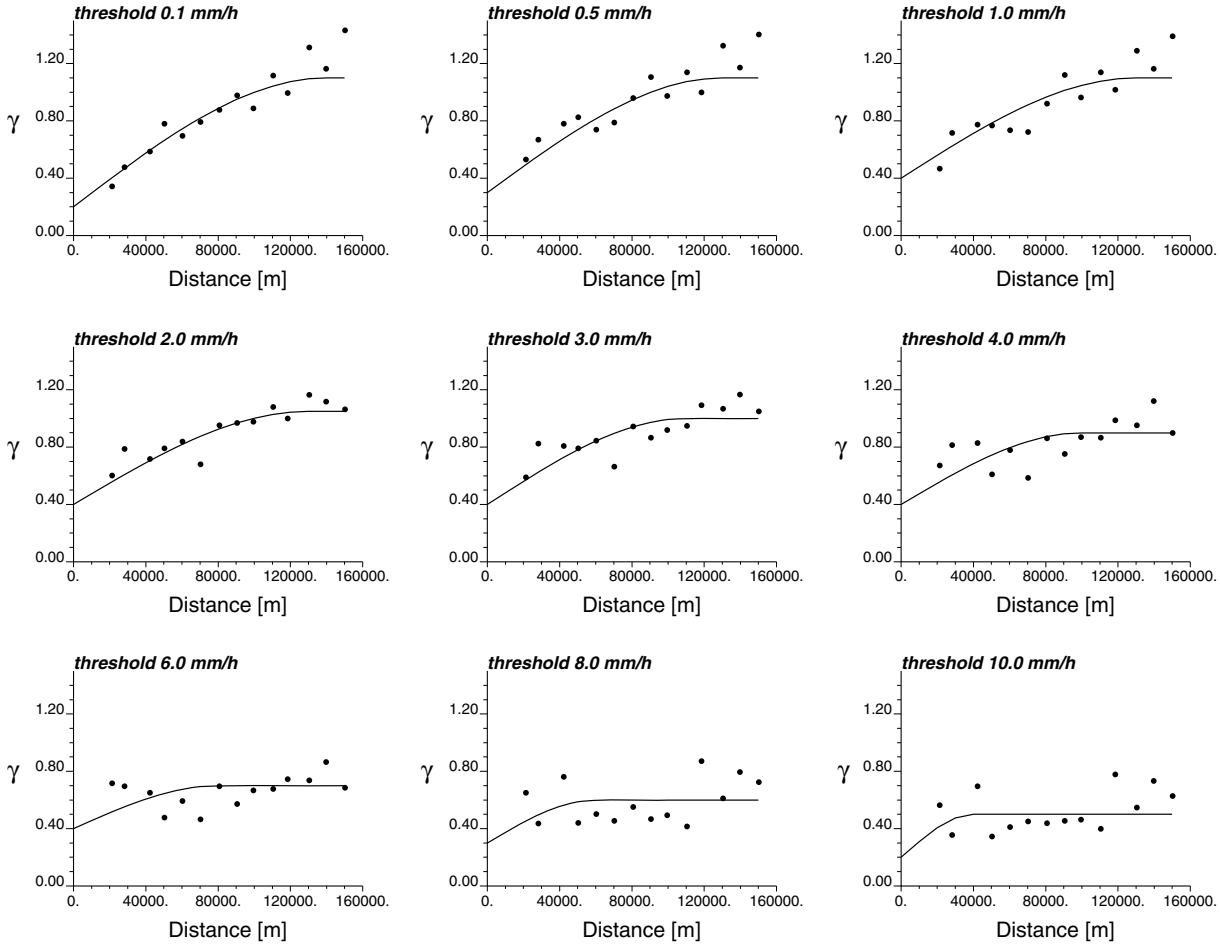

Figure 5 Average standardised indicator variograms for the nine different thresholds characterising hourly rainfall of the extreme storm event.

Table 6 Cross-validation results for interpolation of hourly rainfall without radar information for time steps with $\bar{P} \geqslant 1.0$ mm/h during the period from the 10th to the 13th of August 2002 (averaged over $n = 33$ h)

Method	Bias (mm/h)	RMSE (−)	Cor (−)	RVar (−)
NN	−0.40	1.39	0.26	0.80
IDW	−0.04	1.20	0.34	0.64
OK	0.13	1.12	0.38	0.51
IK	−0.29	1.10	0.41	0.42
KED (El)	0.02	1.11	0.40	0.56
KED (P_{ev})	0.10	0.98	0.54	0.76
KED (El, P_{ev})	0.08	0.98	0.53	0.78
IKED (El, P_{ev})	−0.34	0.98	0.54	0.50

compares the hourly time series of areal precipitation for the subbasin of the Obere Elbe river estimated from station data and radar. This confirms the systematic rainfall underestimation by radar. It also shows the strong variability of the ratio between gauge and radar rainfall rates with values between 2 and 6 within a couple of hours.

Table 7 shows the cross-validation results for interpolation methods with radar as additional information; the first line of the table contains results from a direct comparison of radar data with gauge rainfall (which is not a cross-validation). The negative bias reveals again a strong underestimation of observed rainfall. The high coefficient of correlation, on the other hand, points to a significant relationship between gauge and radar data, which indicates the high potential of radar information as an external drift variable. In the following section, cross-validation results are compared where KED is applied using different additional information but always including radar data. All approaches show better performance than the ones without radar (cp. Table 6). Applying KED with radar rainfall R as the only additional variable results in slightly better performance to that produced if only the event sum P_{ev} is used. Applying IKED with R as the external drift shows a further improvement with respect to the root mean square error and correlation, but results in a higher bias and a smaller variance preservation. Note, that all indicator based methods have a slightly negative bias. This might come from the simplified E-type estimate (see Eq. (10)) with linear interpolation between the thresholds, which leads to an underestimation considering positively skewed distributions. The most significant error reduction is generated when both R and P_{ev} are included into KED as additional information. An extra small gain can be reached

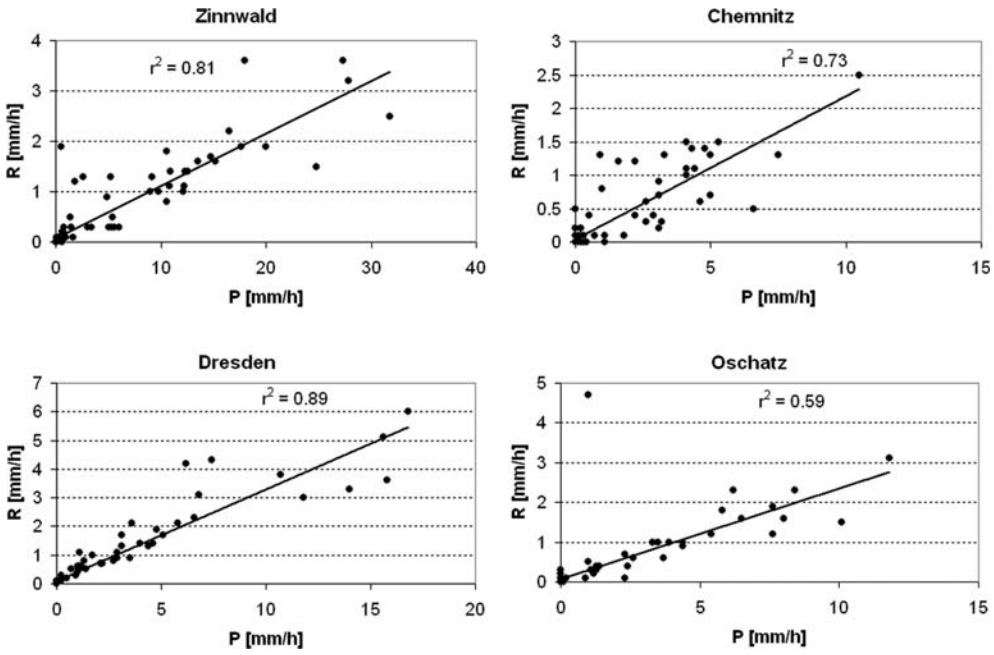

Figure 6 Direct comparison of hourly observed gauge precipitation P with radar derived rainfall rates R at the station grid cells for the total storm period from the 10th to the 13th of August 2002 (r^2 = coefficient of determination).

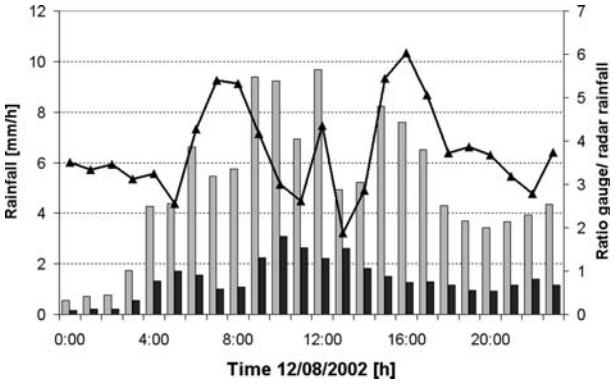

Figure 7 Comparison of hourly areal rainfall for the Obere Elbe subbasin estimated from gauges using KED (P_{ev}) (light grey bars), from radar data only (dark grey bars) and ratio of gauge to radar rainfall (solid line with triangles) for the day 12/08/2002.

Table 7 Cross-validation results for interpolation of hourly rainfall with radar as additional information for time steps with $\bar{P} \geqslant 1.0$ mm/h during the period from the 10th to the 13th of August 2002 (averaged over n = 33 h)

Method	Bias (mm/h)	RMSE (—)	Cor (—)	RVar (—)
Radar only[a]	−2.37	1.33	0.72	—
KED (R)	0.18	1.02	0.61	0.86
IKED (R)	−0.34	0.95	0.65	0.55
KED (R, P_{ev})	0.09	0.86	0.72	0.95
KED (R, P_{ev}, El)	0.11	0.85	0.74	0.96
IKED (R, P_{ev}, El)	−0.39	0.87	0.72	0.57
L-KED (Z, P_{ev}, El)[b]	−0.14	0.79	0.77	0.90

[a] No cross-validation result, but comparison with observed gauge rainfall.
[b] L_KED all variables V involved are log-transformed $\hat{V} = \ln(V + 1.0)$.

when using elevation El as a third external drift variable, which also provides the approach with the best variance preservation ability. Using IKED with all three external drift variables was not found to lead to further improvements compared to KED.

So far only radar rainfall rates R pre-transformed using Eq. (15) have been utilised as external drift here. It is also possible to use the original reflectivity data Z_r instead. A logarithmic transformation of both variables would directly support the assumption made in (1) since rainfall is related to reflectivity non-linearly as expressed in Eq. (15). The cross-validation results from this approach are shown in the last line of Table 7 and after evaluation of the root mean square error and the coefficient of correlation this approach seems best. Although for log-transformed data the estimation is generally biased, the bias here is not very large. Special problems also arise from potentially high uncertainties for extreme values and difficulties considering zero precipitation (Goovaerts, 1997, p. 17; Seo et al., 1990a).

Fig. 8 depicts the spatial distribution of hourly precipitation for two selected hours of the storm event interpolated with three different methods: OK, KED with the rainfall sum P_{ev} as additional information and KED with the three additional variables elevation El, rainfall event sum P_{ev} and radar rainfall R. The application of OK for the interpolation based on the small sample size of only 21 rain gauges clearly creates quite smooth maps. If KED is employed using P_{ev} as external drift, a map with a stronger spatial rainfall structure can be generated, provided the correlation between

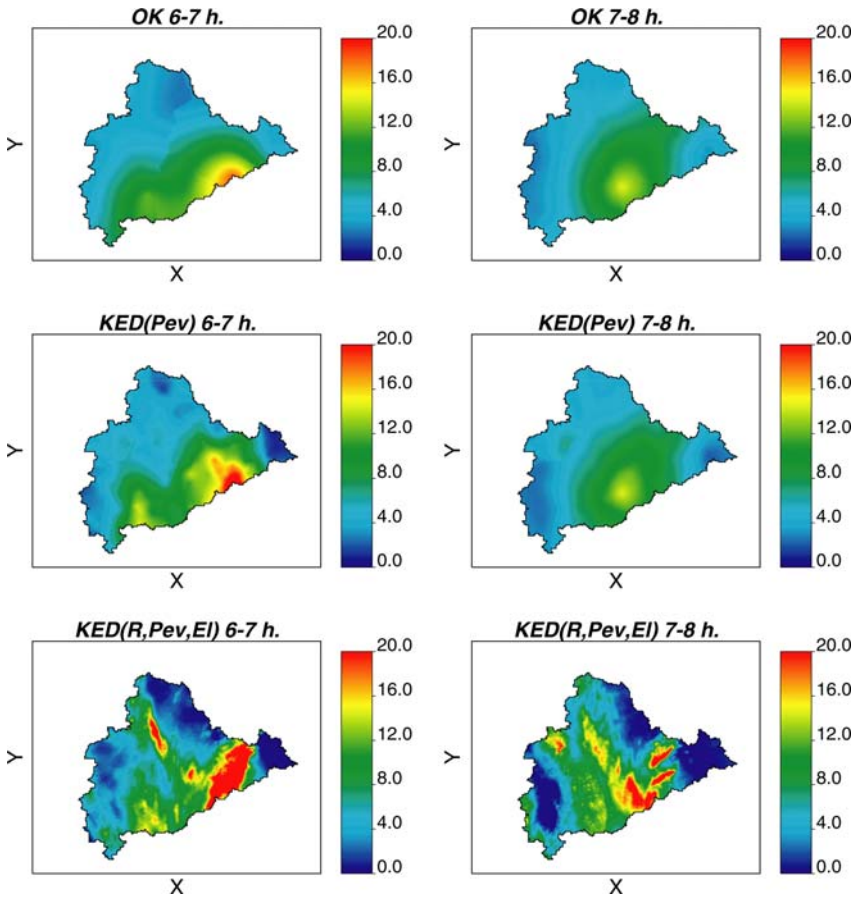

Figure 8 Spatial distribution of precipitation in mm/h for 2 h on the 12/08/2002 interpolated with three different methods: OK, KED with the rainfall sum P_{ev} and KED with the elevation El, the rainfall sum P_{ev} and the radar rainfall rates R as additional information.

primary and additional variables is strong enough. This is the case for the hour from 6:00 to 7:00 a.m. with a correlation of $r = 0.81$. However, the correlation is quite weak ($r = 0.45$) for the other selected hour from 7:00 to 8:00 a.m., so the map looks very much like the smooth map generated using OK. Applying KED with all additional information from radar data R, event sum P_{ev} and elevation El together improves the spatial representation of rainfall significantly. The maps show stronger rainfall variability, higher extremes and typical anisotropic patterns. The multiple correlations between gauge precipitation P and the additional three variables for the first and second selected hour were here 0.91 and 0.68, respectively.

Conclusions

In this study, different geostatistical approaches were compared for the interpolation of hourly precipitation using additional information from radar data, a daily station network and topography. The heavy storm period in the Elbe river basin from the 10th to the 13th of August 2002 was used to illustrate the methods. The focus was on the optimal combination of gauge and radar data using kriging with external drift and indicator kriging with external drift. Special attention was given to the impact of the variogram estimation approach on the interpolation performance. The main results can be summarized as follows:

1. The multivariate methods KED and IKED clearly outperform the univariate ones. The most important additional information is radar followed by precipitation from the denser daily network. The information content of elevation for interpolation of hourly data plays only a minor role here. Using all additional information simultaneously with KED gives the best performance. For some approaches IKED provides smaller root mean square errors than KED, but at the expense of a significant loss of variance.
2. The impact of the semivariogram on interpolation performance is not very high. Although anisotropy is clearly present in the data, no significant differences in prediction performance between isotropic and anisotropic variograms could be found. The best results are obtained using an automatic fitting procedure with isotropic variograms either from hourly or radar data. Cross-validation has shown that the error increases only slightly when using an averaged variogram instead. However, it is not recommended to estimate an averaged variogram based on data with different time steps than those used for interpolation.

3. The exclusive use of uncalibrated radar data cannot be recommended, because this results in a significant underestimation of precipitation. This underestimation is very variable in space and time, which must be taken into account for a useful application of radar information.

This study was conducted based on data from one large-scale extreme rainfall event with hourly discretisation in time. So, it cannot be supposed, that the specific findings will hold in general for any other event, time discretisation or region. However, it is assumed that the main results are valid for a wider range of conditions. With regard to the enumerated points above, it is likely that the degree of generality decreases in the order of points 3, 1, and 2. On the whole it can be concluded that kriging with external drift is a promising method for the interpolation of hourly precipitation using radar data as additional information. Of particular interest is its capability to allow the relationship between primary and secondary variables to change across the study area, since the coefficients of the linear relationship are re-estimated within each local search window. Thus, KED can consider the high space–time variability of the Z–R relationship between radar and gauge rainfall. Efforts are under way to extend the investigations using additional techniques and considering a series of extreme events for different regions and with different time resolutions. The validation of interpolated precipitation using hydrological modelling is also planned for the future. The proposed approaches assume that the gauge rainfall reflects the reality and that point station data can be compared directly with areal radar information. Both assumptions lead to uncertainties, which are not quantified here. Subsequent work should also look for approaches that minimise or remove these restrictive assumptions.

Acknowledgements

This research was partially funded by the State of Saxony. Precipitation and radar data were kindly provided by the German Weather Service (DWD). The author thanks two anonymous reviewers, whose comments helped to improve the paper considerably.

References

Ahmed, S., De Marsily, G., 1987. Comparison of geostatistical methods for estimating transmissivity using data on transmissivity and specific capacity. Water Resources Research 23 (9), 1717–1737.

Bárdossy, A., 1993. Stochastische Modelle zur Beschreibung der raum-zeitlichen Variabilität des Niederschlages. Mitteilungen, 44. Institut für Hydrologie und Wasserwirtschaft, Universität Karlsruhe, Karlsruhe, p. 153.

Cressie, N., 1985. Fitting variogram models by weighted least squares. Mathematical Geology 17, 563–586.

Demyanov, V., Kanevski, M., Chernov, S., Savelieva, E., Timonin, V., 1998. Neural network residual kriging application for climatic data. Journal of Geographic Information and Decision Analysis 2 (2), 215–232.

Deutsch, C.V., Journel, A.G., 1992. GSLIB: Geostatistical software library and user's guide. Oxford University Press, New York, p. 340.

Dubois, G., Malczewski, J., Cort, M.D. (Eds.), 1998. Spatial Interpolation Comparison 97. Journal of Geographic Information and Decision Analysis 2 (1–2)(Special Issue).

DWD, 2002. AKORD – Anwenderkoordinierte Organisation von Radar-Daten, Produktkatalog. Deutscher Wetterdienst, Geschäftsfeld Hydrometeorologie.

Ehret, U., 2002. Rainfall and flood nowcasting in small catchments using weather Radar. Dissertation, Mitteilungen des Instituts für Wasserbau, Heft 21, Stuttgart.

Fassnacht, S.R., Soulis, E.D., Kouwen, N., 2003. Radar precipitation for winter hydrological modelling, Weather radar information and distributed hydrological modelling. IAHS, 35–42, Publication No. 282.

Goovaerts, P., 1997. Geostatistics for natural resources evaluation. Oxford University Press, New York, Oxford, p. 483.

Goovaerts, P., 2000. Geostatistical approaches for incorporating elevation into the spatial interpolation of rainfall. Journal of Hydrology 228 (1–2), 113–129.

Grimes, D.I.F., Pardo-Iguzquiza, E., Bonifacio, R., 1999. Optimal areal rainfall estimation using raingauges and satellite data. Journal of Hydrology 222, 93–108.

Haberlandt, U., Kite, G.W., 1998. Estimation of daily space–time precipitation series for macro-scale watershed modelling. Hydrological Processes 12 (9), 1419–1432.

Hevesi, J.A., Flint, A.L., Istok, J.D., 1992a. Precipitation estimation in mountainous terrain using multivariate geostatistics. Part I: structural analysis. Journal of Applied Meteorology 31, 661–676.

Hevesi, J.A., Flint, A.L., Istok, J.D., 1992b. Precipitation estimation in mountainous terrain using multivariate geostatistics. Part II: Isohyetal maps. Journal of Applied Meteorology 31, 677–688.

Huang, Y., Wong, P., Gedeon, T., 1998. Spatial interpolation using fuzzy reasoning and genetic algorithms. Journal of Geographic Information and Decision Analysis 2 (2), 204–214.

Hutchinson, M.F., 1998a. Interpolation of rainfall data with thin plate smoothing splines: I Two dimensional smoothing of data with short range correlation. Journal of Geographic Information and Decision Analysis 2 (2), 139–151.

Hutchinson, M.F., 1998b. Interpolation of rainfall data with thin plate smoothing splines: II Analysis of topographic dependence. Journal of Geographic Information and Decision Analysis 2 (2), 152–167.

Isaaks, E.H., Srivastava, R.M., 1989. Applied Geostatistics. Oxford University Press, New York.

Krajewski, W.F., Smith, J.A., 2002. Radar Hydrology: rainfall estimation. Advances in Water Resources 25 (8–12), 1387–1394.

Lloyd, C.D., 2005. Assessing the effect of integrating elevation data into the estimation of monthly precipitation in Great Britain. Journal of Hydrology 308 (1–4), 128.

Neary, V.S., Habib, E., Fleming, M., 2004. Hydrologic Modeling with NEXRAD Precipitation in Middle Tennessee. Journal of Hydrologic Engineering 9 (5), 339–349.

Press, W.H., Flannery, B.P., Teukolsky, S.A., Vetterling, W.T., 1989. Numerical Recipes in Fortran 77: The Art of Scientific Computing. Cambridge University Press, New York.

Rudolf, B., Rapp, J., 2003. Das Jahrhunderthochwasser der Elbe: Synoptische Wetterentwicklung und klimatologische Aspekte, Klimastatusbericht 2002. Selbstverlag des Deutschen Wetterdienstes, Offenbach, pp. 172–187. Available from: <http://www.ksb.dwd.de>.

Seo, D.-J., 1998. Real-time estimation of rainfall fields using rain gauge data under fractional coverage conditions. Journal of Hydrology 208, 25–36.

Seo, D.-J., Krajewski, W.F., Bowles, D.S., 1990a. Stochastic interpolation of rainfall data from raingauges and radar using co-kriging: 1. Design of experiments. Water Resources Research 26 (3), 469–477, 89WR02984.

Seo, D.-J., Krajewski, W.F., Bowles, D.S., 1990b. Stochastic interpolation of rainfall data from raingauges and radar using co-kriging: 2. Results. Water Resources Research 26 (5), 915—924, 89WR02992.

Tetzlaff, D., Uhlenbrook, S., 2005. Effects of spatial variability of precipitation for process-orientated hydrological modelling: results from two nested catchments. HESSD 2, 119—154.